PROCEEDINGS OF SPIE

Nonlinear Optics and Applications III

Mario Bertolotti
Editor

20–22 April 2009
Prague, Czech Republic

Sponsored by
SPIE *Europe*

Volume 7354

SPIE

Invited Paper

Mapping of attosecond ionization dynamics by recollision-free higher-order harmonic generation

Aart. J. Verhoef[a], Alexander Mitrofanov[a], Evgenii E. Serebryannikov[b], Daniil V. Kartashov[a], Aleksei M. Zheltikov[b], Andrius Baltuška*[a]
[a]Institut für Photonik, Technische Universität Wien, Gusshausstraße 27-29/387, 1040 Wien, Austria;
[b]Physics Department, International Laser Center, M.V. Lomonosov Moscow State University, Vorobyevy gory, 119992 Moscow, Russia

ABSTRACT

In the presence of a high-intensity optical field, electrons are released from atoms on an attosecond time scale. Moreover, in the tunnelling regime, this process displays a strong sensitivity to the carrier-envelope phase (CEP) of a few-cycle light pulse. Tunnelling ionization – a fascinating quantum mechanical phenomenon – leads to a quasi-stepwise increase of free electron density and, as a consequence, of the refractive index of the medium. These steps of the refractive index, corresponding to half-cycles of the driving optical field, impose a transient attosecond phase mask. By scattering probe light off this mask we detect quasi-periodic higher-order harmonics, the spectrum of which, unlike that of the harmonics originating from intrinsic nonlinearity or driven by electron re-collisions, do not depend on the probe intensity and re-collision dynamics. The implemented noncollinear pump–probe experimental technique allows optical harmonics generated due to a tunnelling-ionization-induced modulation of the electric current to be spatially separated from the harmonics originating from atomic and ionic nonlinear susceptibilities, enabling background-free time-resolved detection of electron-tunnelling-controlled harmonic spectra and offering an attractive solution for attosecond optical metrology of gases and bulk solids.

Keywords: Attosecond, tunnelling ionization, harmonic generation, ultrafast dynamics

1. INTRODUCTION

Tunnelling of an electron through a potential barrier suppressed by a high-intensity light field is a key elementary event that launches a broad diversity of light-induced physical phenomena, turning on the clock in an ultrafast light–matter interaction. Attosecond technologies [1] offer unique tools to resolve the readings of this clock through a direct detection of charged particles [2]. Generation of higher-order harmonics of a light field, taking place in the regime of high-field nonlinear optics [3,4], is one of the cornerstones of attosecond science and technology [1], serving as a tool to synthesize attosecond electromagnetic field waveforms [5], probe molecular orbitals [6], and control attosecond electron dynamics [7]. The physical mechanism behind high-order harmonic generation in the high-field regime, as insightfully explained by Corkum [8], involves ionization of an electron by a strong laser field and subsequent rescattering of this electron by a parent ion. This scenario of harmonic generation is radically different from the harmonic-generation mechanisms known in classical, weak-field nonlinear optics, where the generation of optical signals is described perturbatively in terms of optical nonlinear susceptibilities [4,9]. The Corkum model excellently describes experimentally measured plateau and cutoff higher-order harmonics and provides an important insight into the physics behind strong-field–matter interactions [3].

In the regime of tunnelling ionization, an additional, physically different mechanism of optical harmonic generation is also possible. As shown by Brunel [10], with the ionization rate following the generic law of electron tunnelling through a potential barrier in the dc limit, the plasma density displays extremely fast, nearly stepwise variations at every half-cycle of the laser field, making the plasma current emit odd harmonics of the incident field. Detection of this type of nonlinear-optical response under the conditions of a typical intense-field–gas interaction experiment is very challenging, because the Brunel-type signal is buried under the Corkum-type harmonics from the electrons re-scattered off their parent ions and the harmonics originating from atomic and ionic susceptibilities. As a result, although some interesting

*baltuska@tuwien.ac.at; phone +43 1 58801 387 49; fax +43 1 58801 387 99; atto.photonik.tuwien.ac.at

Nonlinear Optics and Applications III, edited by Mario Bertolotti, Proc. of SPIE Vol. 7354, 73540U · © 2009 SPIE · CCC code: 0277-786X/09/$18 · doi: 10.1117/12.823475

and important experimental observations of the nonlinear wave mixing due to the Brunel-type modulation of the transverse plasma current have been reported [11,12], this regime of harmonic generation has never been experimentally disentangled from the other regimes of harmonic generation.

In this work, we employ a crossed-beam arrangement of a high-intensity linearly polarized few-cycle pump pulse and a weak cross-polarized probe-pulse for a background-free detection of Brunel-type optical harmonics and demonstrate the potential of this process as a new all-optical attosecond metrology technique. A very attractive feature of the Brunel harmonic emission mechanism is that it is free of the electron recombination step, governing the Corkum-type of harmonic emission [8]. Therefore, harmonic generation by plasma-current modulation due to tunnelling ionization is insensitive to the final state of electrons. The spectrum of harmonics generated in this regime is controlled by attosecond ionization dynamics and can be used to resolve this dynamics on the attosecond time scale.

2. EXPERIMENT AND MODEL

The proposed attosecond mapping technique is based on the tunnelling of electrons from a binding potential of an ionic residue suppressed by a high-intensity optical field acting on the system. When the field intensity is high enough, an electron can tunnel through the field-modified, finite-width potential barrier within a time interval shorter than the field half-cycle. The rate of the electron ionization process, $w(t)$, is controlled by the Keldysh parameter [13] $\gamma = \omega_0 \left(2 m_e I_p\right)^{1/2} \left(eE\right)^{-1}$, where ω_0 is the central frequency of the laser field, E is the field amplitude, I_p is the ionization potential, and e and m_e are the electron charge and mass, respectively. For large values of γ, multiphoton ionization (MPI) dominates the ionization process, with w(t) being insensitive to the phase of the field. For low γ (typically $\gamma < 1$), ionisation is dominated by electron tunnelling. In this regime, the ionization rate $w(t)$ becomes highly sensitive to the phase of the field, peaking at the instants of time when the field intensity reaches its maximum. As a result, the electron density displays a steplike temporal profile, with each step being locked to a respective field half-cycle (blue curve, Fig. 1, left). Such a behaviour of $n_e(t)$ has been known from the earlier theoretical work (see Refs. 3,

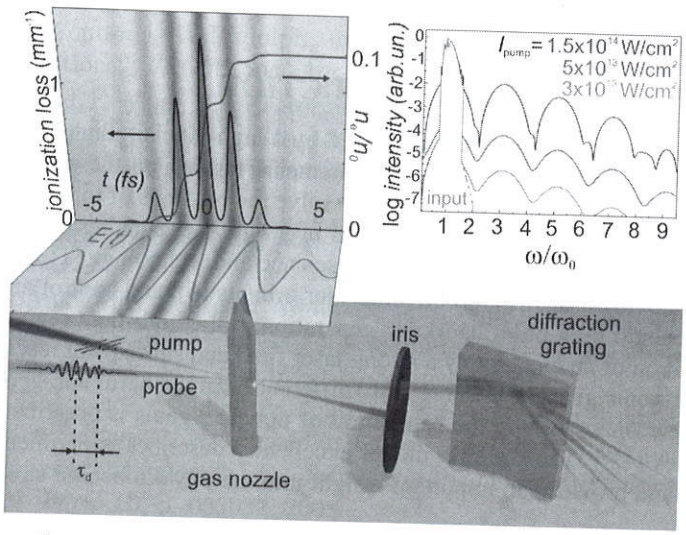

Fig. 1. **All-optical detection of attosecond tunnelling dynamics.** A high-intensity few-cycle pump pulse with a frequency ω_0 (its instantaneous intensity $[E(t)]^2$ is shown by red stripes in the left panel) modulates the electron density through tunnelling ionization. The temporal profiles of the electron density and ionization-induced loss in krypton at 300 mbar in the presence of a pump field with an intensity of $1.5 \cdot 10^{14}$ W/cm^2 are shown by the blue and black solid lines in the left panel. A weak noncollinear probe pulse applied with a variable time delay with respect to the pump (the field in this pulse is shown by the green curve in the left panel) reads out the pump-induced modulation of the plasma current, giving rise to harmonic emission exactly along the probe-beam direction. With an increase of the field intensity, electron tunnelling probability becomes higher, giving rise to a broader harmonic spectrum. The right panel displays the input laser field (dashed line) and the probe field with harmonics generated through plasma current modulation in the presence of a pump pulse with different intensities (encoded by different colors).

14 for an overview) and has been recently visualized experimentally in an elegant time-of-flight spectrometry measurement [2], where attosecond steps in the ion yield were detected using an isolated XUV attosecond pump pulse and a few-cycle optical probe. We observe here that, in the spectral domain, a stepwise modulation of the electron density is manifested as optical harmonic generation (see Fig. 1, right). The spectrum of harmonics emitted in this regime is controlled by attosecond ionization dynamics, thus representing a map of electron tunnelling. With an increase of the field intensity, the Keldysh parameter decreases, and electron tunnelling becomes faster. This, in turn, makes the steps in $n_e(t)$ steeper, mapping faster electron tunnelling onto a broader harmonic spectrum (Fig. 1, right). This mapping suggests the way for an all-optical tracing of attosecond electron tunnelling dynamics.

2.1 Laser system

The laser system used for the experiments is a modified Femtopower Compact Pro Ti:Sapphire chirped pulse amplifier, delivering 700-μJ 25-fs 780-nm pulses, at a repetition rate of 5 kHz. These pulses are spectrally broadened in a neon filled hollow fiber with 250 μm core diameter, and subsequently compressed using broadband chirped mirrors. The neon pressure in the hollow fiber is roughly 3 bar. The 0.5 mm thin antireflection (AR) coated input window of the fiber cell is located about 0.5 m from the fiber input, in order to minimize the nonlinearity in the input window. The 0.5 mm output window has a broadband AR coating, and is located 30 cm after the fiber end. After the hollow fiber, the pulses are recollimated using a spherical silver mirror (ROC=-1.5m), and silver mirrors are used to steer the beam to the experimental setup. A pair of wedges in the beam path are used for fine tuning of the dispersion, in order to minimize the pulse duration in the experiment. The chirped mirror compressor is built in a vacuum chamber, in order to minimize accumulation of non-linear phase of the compressed pulses. An autocorrelator is used to to monitor the pulse duration of the compressed pulses. In the inset of Fig. 2 a typical autocorrelation is shown, together with a typical spectrum at the output of the hollow fiber. A sketch of the laser system and experimental setup is shown in Fig. 2.

2.2 Pump-probe setup

The experimental vacuum chamber is directly flanged to to the vacuum chamber housing the chirped mirror compressor (see Fig. 2). In order to compensate for the material thickness of the beamsplitters used in the experimental setup, the pulses at the entrance of the experimental vacuum chamber are slighly negatively chirped. A flat parallel fused silica plate of which the first surface is uncoated and the second surface has a broadband anti-reflection coating is used as a beam splitter under an angle of ~10 degrees to split off a weak probe beam. After rotating the polarization of the probe beam by 90 degrees with a polarization-rotating periscope (the resulting polarization is vertical), the probe beam is reflected off another (uncoated) flat parallel fused silica plate, this time under an angle of 56 degrees, in order to attenuate the probe beam more. The pump beam is transmitted through this plate, vertically slightly offset from the probe beam, virtually without losses since it is horizontally polarized. The energy of the pump pulses was 250 μJ, and the energy of the probe pulses was about 1 μJ.

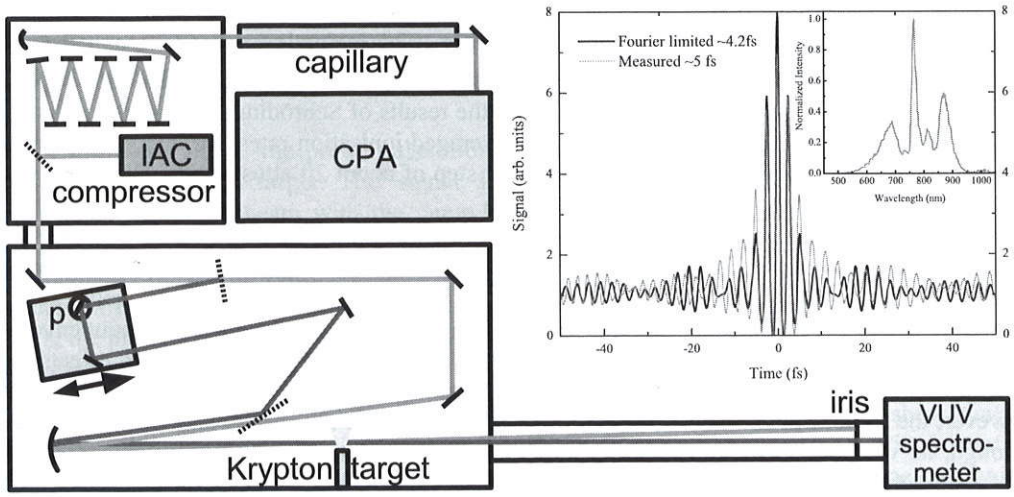

Fig. 2. **Laser system and experimental setup.** The inset shows a typical autocorrelation and spectrum as obtained after compressing the hollow fiber output. IAC – interferometric autocorrelator; CPA – chirped pulse amplifier; p – polarization rotating periscope.

The pump and probe beam are focused into the gas target using a spherical mirror with a focal length of 40 cm. The different gas targets used in our experiment were a 2.5 mm long krypton target, and a 1 mm long argon target. In both cases the neutral gas pressure in the target was 300 mbar. Since the pump and probe beam are slightly vertically offset on the focusing mirror, the beams cross under an angle of about 1.5 degrees in the gas target. Because the pump pulses were transmitted through more glass than the probe pulses, the probe pulses were slightly negatively chirped on target, having a duration of about 10 fs.

2.3 Numerical model

To model the evolution of few-cycle pulses (pump and probe light fields E_{pu} and E_{pr}) in a rapidly ionising gas, we use the pulse evolution equation written in the framework of the slowly evolving wave approximation [3,15] and adapted to include ionization effects [16,17]. In this model, we include gas and plasma dispersion, diffraction, spatial self-action induced by the Kerr nonlinearity of the gas and plasma nonlinearity, spectral transformation phenomena, including self-phase modulation, wave mixing and harmonic generation, shock-wave effects, as well as ionization-induced loss and plasma-related nonlinear phenomena. The ionisation rate $w(t)$ is calculated by using the Yudin–Ivanov formula [18]. We numerically solve the following evolution equation for the total field $E = E_{pu} + E_{pr}$:

$$\frac{\partial E}{\partial z}(z,r,\omega) = i\left(k(\omega) - \frac{\omega}{V_g}\right)E(z,r,\omega) + i\frac{\chi^{(3)}_{THG}}{2k(\omega)}\hat{F}\left(E^3(z,r,t)\right) -$$

$$-\frac{1}{2}\hat{F}\left[\left(\alpha - \frac{I_p}{I_0\left|E(z,r,t)\right|^2}\cdot\frac{\partial n_e}{\partial t}\right)E(z,r,t)\right] + i\frac{1}{2\omega c}\hat{F}\left(\omega_p^2(z,r,t)A(z,r,t)\right) + \qquad (1)$$

$$+i\frac{1}{2k(\omega)}\left[\frac{\partial^2}{\partial r^2} + \frac{\partial}{r\partial r}\right]\hat{F}\left(E(z,r,t)\right)$$

Here, $E(z,r,\omega) = \hat{F}^{-1}\left(\sqrt{I_0}A(z,r,t)\cdot\exp(i\omega_0 t) + c.c.\right)$, $\hat{F}(\bullet)$ is the Fourier transform operator, I_0 is the peak field intensity, $A(z, r, t)$ is the field envelope, z and r are the longitudinal and radial coordinates, respectively, ω is the radiation frequency, V_g is the group velocity, $\chi^{(3)}_{THG}$ is the third-order susceptibility responsible for third-harmonic generation, α is the attenuation coefficient, $\omega_p(z,\tau) = \left[4\pi e^2 n_e(z,\tau)/m_e\right]^{1/2}$ is the plasma frequency, and n_e is the electron density. Dispersion of the gas medium is plugged into Eq. (1) through the frequency profile of the wave number $k = k(\omega)$, which automatically includes high-order dispersion effects.

The electron density n_e created in the gas by a laser field was calculated by solving the kinetic equation $\partial n_e/\partial t = w(n_0 - n_e)$, where n_0 is the density of neutral species. The ionization rate $w(t)$ was calculated using the Yudin–Ivanov formula [18], which provides a compact closed-form analytical expression for the ionisation rate, which is valid within a broad range of field intensities, agrees well with the results of Schrödinger-equation analysis of ionization [2], and reproduces Keldysh-type expressions [13] for cycle-averaged ionisation rates. Eq. (1) was solved by using the Split-Step Fourier method on a time gate of 500 fs with a time step of about 20 attoseconds. Discretisation steps along the longitudinal and radial coordinates were taken equal to 1 μm.

In Fig. 3, we present the results of simulations performed for ultrashort pump and probe pulses interacting with a 1 mm argon gas jet with a neutral gas pressure of 300 mbar. The pump pulse with an initial pulse width of about 5 fs and an energy of 250 μJ induces an ultrafast modulation of the electron density in the gas, acquiring well-resolved amplitude modulation due to the rapidly varying plasma loss (the inset in Fig. 3). The probe pulse with an input envelope shown by the dashed line reads out the amplitude and phase masks induced by the pump field. Propagation effects complicate the retrieval of the information on attosecond electron tunnelling dynamics from the time-resolved harmonic spectra of the probe field. However, the signatures of electron tunnelling in the temporal of the probe pulse transmitted through the gas jet are clear enough, as visualized by the oscillatory structure in the central part of the pulse in Fig. 3, to allow the reconstruction of spatiotemporal maps of ionisation rate and electron density build-up.

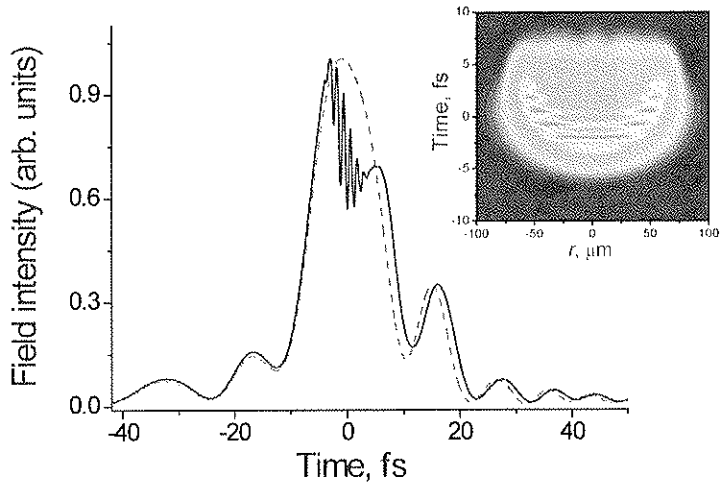

Fig. 3. **Signatures of electron tunnelling in the transformation of an ultrashort probe pulse in a gas ionised by a high-intensity pump.** Temporal envelopes of the input probe pulse and the probe pulse transmitted through the argon gas jet with parameters specified in the main text are shown by the dashed and solid lines, respectively. An ultrafast modulation of the electron density in the gas jet is induced by a pump field with an initial pulse width of about 5 fs and an energy of 250 μJ. Temporal envelope of the pump pulse transmitted through the gas jet is presented in the inset.

3. RESULTS

3.1 Harmonic generation in Krypton and Argon

A high-intensity few-cycle pump pulse with a frequency ω_0 modulates the electron density through tunnelling ionization and a very weak probe pulse at the same or other optical frequency reads out the pump-induced modulation of the plasma current. In this noncollinear pump–probe scheme, the Corkum-type harmonics, emitted in the pump beam direction, are spatially separated from harmonics generated due to plasma density modulation, since these latter harmonics are emitted in the direction of the probe beam. By varying the pump–probe delay τ_d we are also able to discriminate between any possible background signal due to atomic/ionic nonlinear susceptibilities and the readout of the phase modulation signature related to tunnelling ionization in the probe beam direction. By detecting the signal strictly in the probe direction, we, in addition, dismiss contamination from sum- and difference-frequency beams, because their phase-matched directions lie, correspondently, inside and outside the pump–probe non-collinearity angle. With this arrangement, we could reliably detect and perform reproducible frequency- and time-resolved measurements on the third, fifth, and seventh harmonics emitted from krypton and argon gas jets in the direction of the probe beam (Figs. 4a – 4d and 5a).

In the absence of the pump pulse, the probe pulse alone could also generate the third harmonic due to the atomic nonlinear susceptibility of the gas target. This signal, however, noticeably differed in its properties from the third harmonic generated by the probe beam with the pump field on. While in the presence of the pump field, the third harmonic scaled approximately linearly with the probe energy (black line in Fig. 5c), when the pump field was turned off, the third harmonic closely followed the scaling $(W_{pr})^3$ with the energy W_{pr} of the probe field (red line in Fig. 5c), indicating a change in the mechanism behind harmonic generation. In time- and frequency-resolved measurements on optical harmonics, the probe energy was chosen such that harmonic signals contained no or very low background due to the atomic nonlinear susceptibilities of the gas target.

The predictive power of our numeric model model is illustrated by Figs. 5a – 5c, which show that the results of simulations agree very well with the experimental data for the spectral and temporal properties of optical harmonics (Figs. 5a, 5b), as well as for the behaviour of the third-harmonic signal as a function of the probe energy in the presence and in the absence of the pump field (Fig. 5c).

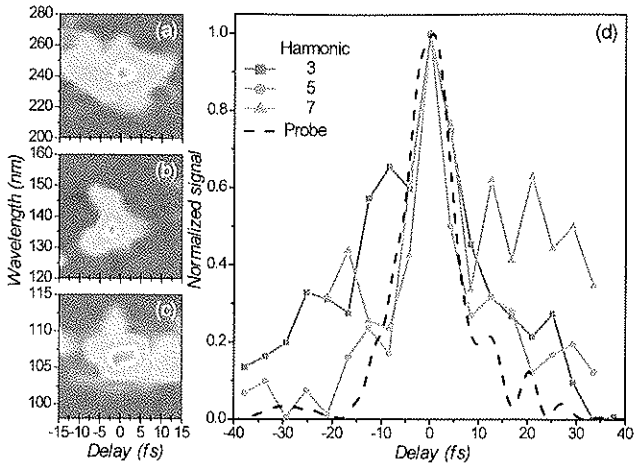

Fig. 4. **Spectrally resolved and spectrally integrated time dependence of optical harmonics from a krypton jet.** (a - c) Experimental maps of the third (a), fifth (b), and seventh (c) spectrally resolved harmonics of the probe beam detected as a function of the delay time τ_d between the pump and probe pulses. (d) The spectrally integrated harmonic signals as a function of the delay time τ_d all show the same temporal structure. The measured time-dependent signal agrees well to the calculated probe intensity envelope (dashed line). The pump pulse with an initial pulse width of 5 fs and an energy of 250 μJ is focused by a lens with a focal length of 40 cm in a krypton jet with a gas pressure of 300 mbar.

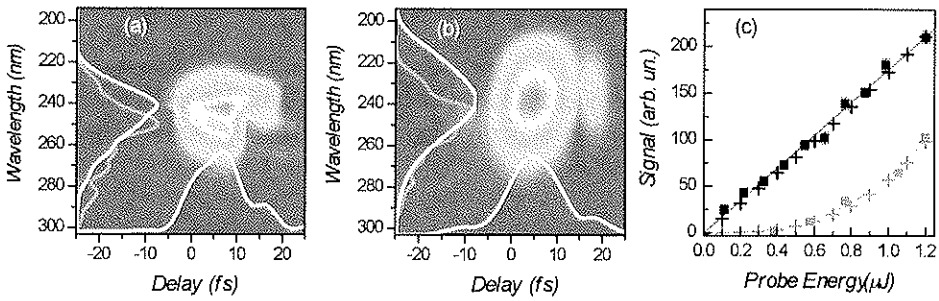

Fig. 5. **The third harmonic from an argon jet: measurements versus simulations.** The third-harmonic signal from a 1 mm long argon target with a neutral gas pressure of 300 mbar. Panel (a) shows the experimentally measured spectrogram, with the time integrated signal collapsed on the spectral axis, and the spectrally integrated signal collapsed on the delay axis (yellow lines). The signal below 220 nm is absorbed before the spectrometer. The grey line shows the normalized spectrum of the third harmonic in the absence of the strong pump pulse. Panel (b) shows the simulated spectrogram, with the spectrally and time integrated signals collapsed on the delay and wavelength axes respectively (yellow lines). The grey line shows the numerically obtained normalized third harmonic signal in the absence of the pump. Panel (c) shows the third harmonic signal measured (squares) and simulated (+) as a function of the probe energy in the presence of the strong pump pulse (black) and in the absence of the strong pump (red).

One of the main difficulties to apply the harmonic pump-probe technique on transparent glasses is a much narrower transparency region in comparison with gases, because harmonic orders higher than the 3rd (for the fundamental wavelength of ~800 nm) are absorbed by the sample. To maximize the amount of spectral peaks corresponding to Brunel wave-mixing [12] products, we have applied a two-color pump-probe permitting generation of non-degenerate $N\cdot 2\omega_{pump}\pm\omega_{probe}$ ($N\in$integer) frequency components. An example of a two-color experiment is given in Fig. 6, showing that the signal at the frequency $2\omega_{pump}+\omega_{probe}$ in Fig.1b is purely caused by the stepwise change of the refractive index in time (phase mask in Fig.1a), because a circularly polarized pump field does not produce ionization steps. The lifting of degeneracy permits a clear separation of the TI response from a strong background of sum frequency components (e.g. $\omega_{pump}+2\omega_{probe}$, Fig. 6b) occurring when the pump and probe polarizations are not orthogonal.

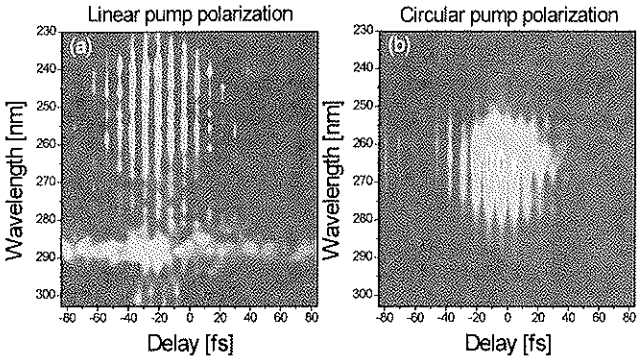

Fig. 6. **Brunel mixing with non degenerate pump and probe wavelength.** Measured cross-correlations for the third harmonic for linearly polarized (b) and circularly polarized (c) pump fields corresponding, respectively, to a stepwise (b) and a smooth (c) phase masks. Panel (c) clearly shows suppression of the Brunel-type signal and appearance of a wave-mixing maximum due to non-orthogonal pump and probe fields. The cross-correlation traces in both (b) and (c) clearly exhibit optical fringes caused by the smallness of the non-collinearity angle between the pump and the probe beams.

For an adequate explanation of how the information on attosecond electron tunnelling dynamics is encoded in the spectral–temporal structure of harmonics, we distinguish between two physical mechanisms. The first mechanism involves the pump-induced plasma loss, proportional to $\alpha_p \propto I_p \partial n_e/\partial t$ (see Eq. (1)), which maps the temporal profile of $\partial n_e/\partial t$ onto the transmission of the probe field. Thus, in the regime of tunnelling ionization, probe transmission becomes a pump-phase-sensitive pulsating function of time (black curve in Fig. 1, left), imposing an ultrafast, $\propto \partial n_e/\partial t$ amplitude modulation on the laser pulse (see the insets in Fig. 4b and Fig. 3), giving rise to odd-order harmonics of ω_0 in the spectrum of the probe field. The second mechanism is related to the nonlinear phase shift $\Delta\Phi = \omega_0 \delta n_p \Delta z/c$ of the probe field induced by an ultrafast modulation of the plasma current within a small propagation length Δz, with c being the speed of light in vacuum, $\delta n_p \approx -\omega_p^2/\left(2\omega_0^2\right)$, ω_p being the plasma frequency. Since $\omega_p^2 \propto n_e(t)$, this phase mask follows the temporal profile of $n_e(t)$. With $n_e(t)$ displaying stepwise changes locked to oscillations of the pump field, this mechanism also gives rise to peaks at the frequencies of odd harmonics of ω_0 in the spectrum of the probe field (Fig. 1, right).

For the conditions of the experiments presented here, both amplitude and phase modulation of the probe field in a tunnelling-ionizing gas play a non-negligible role in harmonic generation. Propagation effects generally tend to blur the steps in the electron-density buildup sensed by the probe pulse, thus complicating the map between the electron tunnelling dynamics and time-resolved harmonic spectra of the probe field (Fig. 7a). Still, the probe pulse transmitted through the pump–probe interaction region displays well-resolved amplitude modulation due to the rapidly varying plasma loss (Fig. 3). This allows the information on the dynamics of electron tunnelling to be retrieved from the numerical model adjusted to provide the best fit for time-resolved harmonic maps and other properties of optical harmonics measured in noncollinear pump–probe experiments geometry (Figs. 5a – 5b). Figure 6a presents the spatiotemporal map of the ionisation rate along the argon jet that provides the best fit (Fig. 5b) for the experimental third-harmonic maps (Fig. 5a) and, in addition, explains very well the dependence of the third-harmonic signal on the energy of the probe pulse with and without the pump field (Fig. 5c). In the central, most intense part of the laser pulse, the peaks in the time dependence of the ionisation rate in Figs. 7a and 7b, become as narrow as 350 attoseconds, giving rise to attosecond steps in the temporal profile of the electron density (Fig. 7b), which translate into ultrafast modulation features on both pump and probe pulses (see Fig. 3).

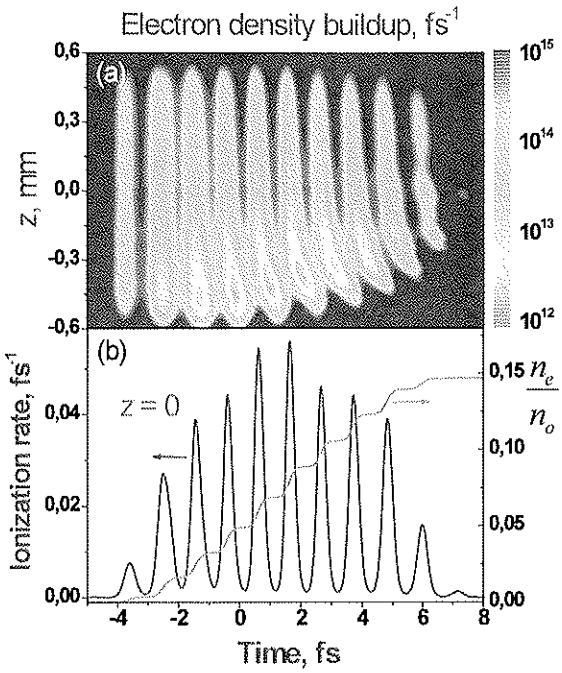

Fig. 7. **Retrieval of electron tunnelling dynamics.** (a) Spatiotemporal map of the ionisation rate along the argon jet providing the best fit for the experimental third-harmonic maps (Figs. 5a, 5b). (b) Time dependences of the ionisation rate and the normalized electron density at the centre of the gas jet ($z = 0$) on the beam axis.

4. CONCLUSIONS

In conclusion, we demonstrated an all-optical method enabling the detection of attosecond electron tunnelling dynamics based on optical harmonic generation due to an ultrafast modulation of the plasma current in a fast-ionizing gas medium. This approach offers an all-optical alternative to the methods of attosecond metrology based on the detection of charged particles, allowing attosecond spectroscopy and imaging technologies to be extended to the analysis of attosecond electron dynamics in large molecules and bulk solids. We have demonstrated a noncollinear pump–probe experimental technique that enables time-resolved mapping of optical harmonics generated by tunnelling electrons and allows these harmonics to be spatially separated from harmonics originating from atomic and ionic nonlinear susceptibilities.

REFERENCES

[1] P. B. Corkum and F. Krausz, „Attosecond science," Nature Phys. **3**, 381 - 387 (2007).

[2] M. Uiberacker, Th. Uphues, M. Schultze, A. J. Verhoef, V. Yakovlev, M. F. Kling, J. Rauschenberger, N. M. Kabachnik, H. Schroder, M. Lezius, K. L. Kompa, H.-G. Muller, M. J. J. Vrakking, S. Hendel, U. Kleineberg, U. Heinzmann, M. Drescher, and F. Krausz, "Attosecond real-time observation of electron tunnelling in atoms," Nature **446**, 627-632 (2007).

[3] T. Brabec and F. Krausz, "Intense few-cycle laser fields: Frontiers of nonlinear optics," Rev. Mod. Phys. **72**, 545-591 (2000).

[4] A. L'Huillier et al. Nonlinear Optics, in Handbook of Lasers and Optics, ed. by F. Träger, New York, Springer, 2007, pp. 157 – 248.

[5] E. Goulielmakis, M. Schultze, M. Hofstetter, V. S. Yakovlev, J. Gagnon, M. Uiberacker, A. L. Aquila, E. M. Gullikson, D. T. Attwood, R. Kienberger, F. Krausz, U. Kleineberg " Single Cycle Nonlinear Optics" Science, **320** 1614-1617 (2008).
[6] J. Itatani, J. Levesque, D. Zeidler, H. Niikura, H. Pepin, J. C. Kieffer, P. B. Corkum and D. M. Villeneuve, "Tomographic Imaging of Molecular Orbitals", Nature **432**, 867-871 (2004).
[7] A. Baltuska, T. Udem, M. Uiberacker, M. Hentschel, E. Goulielmakis, C. Gohle, R. Holzwarth, V.S. Yakovlev, A. Scrinzi, T.W. Hänsch, and F. Krausz, "Attosecond control of electronic processes by intense light fields," Nature **421,** 611-615 (2003).
[8] P.B. Corkum, "Plasma perspective on strong-field multiphoton ionization," Phys. Rev. Lett. **71**, 1994-1997 (1993).
[9] N. Bloembergen, Nonlinear Optics (Benjamin, New York, 1964).
[10] F. Brunel, "Harmonic generation due to plasma effects in a gas undergoing multiphoton ionization in the high-intensity limit," J. Opt. Soc. Am. B **7**, 521-526 (1990).
[11] N. Burnett, C. Kan, and P.B. Corkum, "Ellipticity and polarization effects in harmonic generation in ionizing neon," Phys Rev A **51**, R3418 - R3421 (1995).
[12] C.W. Siders, G. Rodriguez, J.L.W. Siders, F.G. Omenetto, and A.J. Taylor, "Measurement of Ultrafast Ionization Dynamics of Gases by Multipulse Interferometric Frequency-Resolved Optical Gating," Phys. Rev. Lett. **87**, 263002 (2001).
[13] L. V. Keldysh, "Ionization in the field of a strong electromagnetic wave," Zh. Eksp. Teor. Fiz. **47**, 1945–1957 (1964) [Sov. Phys. JETP **20**, 1307–1314 (1965)].
[14] W.M. Wood, C.W. Siders, and M.C. Downer, "Femtosecond growth dynamics of an underdense ionization front measured by spectral blueshifting," IEEE Trans. Plasma Sci. **21**, 20 – 33 (1993).
[15] T. Brabec and F. Krausz, „Nonlinear Optical Pulse Propagation in the Single-Cycle Regime," Phys. Rev. Lett. **78**, 3282 – 3285 (1997).
[16] L. Bergé, S. Skupin, R. Nuter, J. Kasparian, and J.-P. Wolf, "Ultrashort filaments of light in weakly ionized, optically transparent media," Rep. Prog. Phys. **70**, 1633–1713 (2007).
[17] E. E. Serebryannikov, E. Goulielmakis, and A. M. Zheltikov, "Generation of supercontinuum compressible to single-cycle pulse widths in an ionizing gas," New J. Phys. **10**, 093001 (2008).
[18] G. L. Yudin and M. Yu. Ivanov, "Nonadiabatic tunnel ionization: looking inside a laser cycle," Phys. Rev. A **64**, 013409 (2001).